Electronic Supplementary Material (ESI) for Journal of Materials Chemistry C.

Supporting Information

Rational Design of New Chalcogenide with Good Infrared Nonlinear Optical Performance: $SrZnSnS_4$

Yiling Zhang,[a] Dajiang Mei,*[a] Yi Yang,[bc] Wangzhu Cao,[a] Yuandong Wu,[a] Jie Lu*[a] and Zheshuai Lin*[bc]

[a] College of Chemistry and Chemical Engineering, Shanghai University of Engineering Science, Shanghai 201620, China.

* E-mail: **meidajiang718@pku.edu.cn**

* E-mail: **dr.lujie@foxmail.com**

[b] Technical Institute of Physics and Chemistry, Chinese Academy of Sciences, Beijing 100190, China

* E-mail: **zslin@mail.ipc.ac.cn**

[c] University of Chinese Academy of Sciences, Beijing 100190, China

Contents

Experimental Sections

Solid-state synthesis

The starting reagents were stored in an Ar-filled glove-box without oxygen and moisture. The pure phase sample of $SrZnSnS_4$ was synthesized through high-temperature solid-state reaction. The SrS (99.9%), Zn (99.9%), Sn (99.5%), and S (99.9%) were ground, then loaded into a silica tube coated with carbon in the molar radio of 1: 1: 1: 3, subsequently, sealed under vacuum ($<10^{-3}$ Pa), finally, moved into the computer-controlled muffle furnace with following controlled warming procedure: heated to 800℃ within 30 h, dwelled there for 30 h, and cooled slowly until ambient temperature (6℃/h). At last, the power of $SrZnSnS_4$ was obtained and further tested.

Single crystal growth

The prepared powder of $SrZnSnS_4$ was mixed with flux KI at the ratio of 1: 1, and then the mixtures were loaded into the graphic crucible placed in the silica tube. Next, the tubes were sealed under vacuum ($<10^{-3}$ Pa) and put into a programmed muffle furnace with the following controlled heating ramp: heated to 800℃ within 30 h, kept at this temperature for two days, and slowly cooled to ambient temperature with the speed of 3℃/h. Finally, the title product was cleaned with distilled water to get rid of the redundant KI and the yellow crystals are stable in air.

Poly-crystalline powder X-ray diffraction

The X-ray diffraction analysis of $SrZnSnS_4$ powder was performed on an automated Bruker D2 phaser [Cu Kα (λ = 1.5418 Å)]. The angular scope is 2θ = 10–70° with scanning step of 0.02°. It is satisfied that the powder pattern of $SrZnSnS_4$ is in line with the simulated pattern of single crystal data, indicating the product of title compound is highly purified (Figure S2).

Crystal structure determination

High quality single crystals of $SrZnSnS_4$ were manually picked under an microscope to determinate the crystal structure and the graphite-monochromatized Mo Kα radiation (λ = 0.71073 Å) which is installed in a Rigaku

XtaLAB PRO diffractometer with a Dectris PILATUS detector was used to harvest the single crystal data. SHELX-2014/7 software package was used to resolve and refine the structure by direct method and full-matric least squares fitted on F^2, respectively.[1] The related crystal structure data and specific details are summarized in Table S1.

UV-Vis diffuse reflectance spectroscopy

The UV test of powder $SrZnSnS_4$ was carried out on a Shimadzu UV–3600 spectrophotometer in the scope of 200–1500 nm at ambient temperature and $BaSO_4$ plate was used as a reference.

Second harmonic generation

The second harmonic generation (SHG) response was tested by means of Kurtz and Perry method[2] with the laser of 1.06 μm Q–switched Nd: YAG. The particle size of the test sample was 80–100 μm and the entire procedure was repeated using $LiGaS_2$ served as a reference in the same particle size. Besides, the SHG intensity of $SrZnSnS_4$ was recorded at 1.06 μm radiation.

Computational method

The CASTEP[3] package that is a plane-wave pseudopotential method depended on density functional theory (DFT)[4] was used for the calculated electronic band structure of $SrZnSnS_4$. The exchange-correlation energy was elaborated through the functional developed by the generalized gradient approximation (GGA)[5-6] of Perdew-Burke-Emzerhoff (PBE) form. The valid interactions between atom cores and valence electrons were modeled by means of the optimized norm-conserving pseudopotentials[7] in the Kleinman-Bylander[8] form for total elements. And in the context of without influencing the computational accuracy, Sr $4s^24p^65s^2$, Zn $3d^{10}4s^2$, Sn $5s^25p^2$ and S $3s^23p^4$ electrons were deemed as valence electrons and a correspondingly diminutive basis set was allowed to adopted. A dense 3×3×3 Monkhorst-Pack[5] *k*-point meshes which is in the Brillouin zones and the high kinetic cutoff energy of 900 eV were selected for $SrZnSnS_4$. The test demonstrated that the aforementioned computational set ups are adequately correct for current aims.

As is noted, the exchange-correlation energy is discontinuous, which leads to a result that the measured energy gaps are bigger compared with the calculated ones by standard DFT method. In order to fit the calculated energy gaps with the measured values, all conduction bands were shifted by the scissor operators[6]. Besides, the imaginary part of the dielectric function was computed based on the scissor-corrected electron band structure in light of the electron transition from the valence bands (VB) to conduction band (CB). Therefore, the Kramers-Kronig[9] transform was adopted to determine the real part of the dielectric function

and the refractive indices are obtained. Moreover, the SHG coefficients (d_{ij}) can be determined through the equation proposed by our team.[10]

Bond valance sum (BVS) calculation

Bond valence sum calculation was implemented by following formula[11, 12]:

$$V_{\mathrm{i}} = \sum_{j} S_{ij} = \sum_{j} \exp\left(\frac{R_0 - R_{ij}}{B_0}\right)$$

Table 1. The meaning of symbols in the formula.

V_i	the valence of atom i	S_{ij}	the partial valence of each bond
R_0	the distance of a bond unit valence	B_0	a 'universal' constant with 0.37 Å
R_{ij}	the distance of a bond unit valence and the bond distance between atom i and atom j		

In this work, taking R_0 values for Sr–S (2.59Å), Zn–S (2.09Å) and Sn–S (2.45Å).[13] The results of BVS calculation of $SrZnSnS_4$ show that Sr1 (1.85), Sr2 (1.85), Sr3 (1.87), Zn1 (1.89), Zn2 (1.90), Sn1 (4.62) and Sn2 (4.73), respectively. For comparison and verification of accuracy, the BVS calculation of $BaZnSnS_4$ was carried out with R_0 values for Ba–S (2.77Å)[13] and other related data is agreement with that of $SrZnSnS_4$. The results manifest that Ba1 (2.29), Ba2 (2.29), Ba3 (2.03), Zn1 (1.81), Zn2 (1.82), Sn1 (4.64), Sn2 (4.62). Thus, the valence states in $SrZnSnS_4$ are reasonable.

Table S1. The related crystal structure data and specific details of $SrZnSnS_4$.

	$SrZnSnS_4$
f_w	399.92
a (Å)	12.6336(4)
b (Å)	20.9242(8)
c (Å)	20.8591(9)
Volume (Å^3)	5514.06(40)
Space group	*Fdd*2 (No.43)
Z	32
Index ranges	$-17 \le h \le 17$
	$-26 \le k \le 28$
	$-28 \le l \le 25$
ρ_c (Mg m $^{-3}$)	3.854
μ (mm $^{-1}$)	15.842
R_1, wR_2 [$I > 2$sigma (I)]	0.0415, 0.1411
R_1, wR_2 (all data)	0.0526, 0.1607
Weight = 1 / [sigma^2(F_o^2) + (0.0220 * P) ^2 + 84.95 * P] where P = (Max (Fo^2, 0) + 2 * F_c^2) / 3	

Table S2. Selected bond distances (Å) of $SrZnSnS_4$.

Bond distance	(Å)	Bond distance	(Å)
Sr1–S1×2	3.104(4)	Sn1–S3	2.396(4)
Sr1–S3×2	3.185(4)	Sn1–S4	2.399(4)
Sr1–S4×2	3.131(5)	Sn1–S5	2.439(4)
Sr1–S5×2	3.110(4)	Sn1–S8	2.358(4)
Sr2–S2×2	3.098(3)	Sn2–S1	2.355(4)
Sr2–S6×2	3.151(5)	Sn2–S2	2.408(4)
Sr2–S7×2	3.180(4)	Sn2–S6	2.391(4)
Sr2–S8×2	3.107(4)	Sn2–S7	2.400(4)
Sr3–S1	3.115(4)	Zn1–S5	2.300(5)
Sr3–S2	3.106(4)	Zn1–S6	2.399(4)
Sr3–S3	3.154(4)	Zn1–S7	2.388(4)
Sr3–S4	3.195(4)	Zn1–S8	2.393(4)
Sr3–S5	3.103(4)	Zn2–S1	2.388(4)
Sr3–S6	3.153(4)	Zn2–S2	2.301(4)
Sr3–S7	3.115(4)	Zn2–S3	2.389(4)
Sr3–S8	3.095(4)	Zn2–S4	2.394(4)

Table S3. Selected bond angles (deg) of $SrZnSnS_4$.

Bond angle	(deg)	Bond angle	(deg)
S3–Sn1–S5	107.24(14)	S5–Zn1–S6	125.38(15)
S4–Sn1–S5	106.72(14)	S5–Zn1–S7	125.63(15)
S4–Sn1–S3	96.26(12)	S5–Zn1–S8	101.78(16)
S8–Sn1–S3	121.33(15)	S7–Zn1–S6	97.44(15)
S8–Sn1–S4	121.30(15)	S8–Zn1–S6	101.07(15)
S8–Sn1–S5	102.91(13)	S8–Zn1–S7	100.58(15)
S1–Sn2–S2	103.71(14)	S2–Zn2–S1	101.25(13)
S1–Sn2–S6	123.93(13)	S2–Zn2–S3	122.50(15)
S1–Sn2–S7	123.47(13)	S2–Zn2–S4	121.84(15)
S6–Sn2–S2	102.34(13)	S3–Zn2–S1	106.69(15)
S6–Sn2–S7	97.31(14)	S4–Zn2–S1	106.69(15)
S7–Sn2–S2	102.70(13)	S4–Zn2–S3	96.60(12)

Table S4. Calculated nonlinear optical properties coefficients.

	$SrZnSnS_4$
d_{31}	1.935 pm/V
d_{32}	–4.35 pm/V
d_{33}	–5.91 pm/V

Table S5. The optical properties of $AM^{II}M^{IV}Q_4$ (A = Ba, Sr; M^{II} = Zn, Cd, Hg; M^{IV} = Si, Ge, Sn; Q = S, Se).

Compound	Space group	Band gap (eV)	SHG	Reference
$SrZnSnS_4$	*Fdd*2	2.83	1×$LiGaS_2$	This work
$BaCdSnS_4$	*Fdd*2	2.30	5×$AgGaS_2$[a], 0.7×$AgGaS_2$[b]	14
$SrCdSnS_4$	*Fdd*2	2.05	1.3×$AgGaS_2$	15
$BaCdSnSe_4$	*Fdd*2	1.79	1.6×$AgGaS_2$	16
$SrCdSnSe_4$	*Fdd*2	1.54	1.5×$AgGaS_2$	15
$BaZnSiSe_4$	*Ama*2	2.71	0.3×$AgGaS_2$	17
$SrCdGeS_4$	*Ama*2	2.60	2×$AgGaS_2$	18
$BaHgGeSe_4$	*Ama*2	2.49	4.7×$AgGaS_2$	19
$BaZnGeSe_4$	*Ama*2	2.46	1×$AgGaS_2$	17
$SrHgGeSe_4$	*Ama*2	2.42	4.8×$AgGaS_2$	19
$SrCdGeSe_4$	*Ama*2	1.90	5×$AgGaS_2$	18

[a] The SHG was measured at particle size of 38–55 μm. [b] The SHG was measured at particle size of 150–200 μm.

Figure S1. Diffuse reflectance spectra of $SrZnSnS_4$ through direct extrapolation method with baseline tangent.

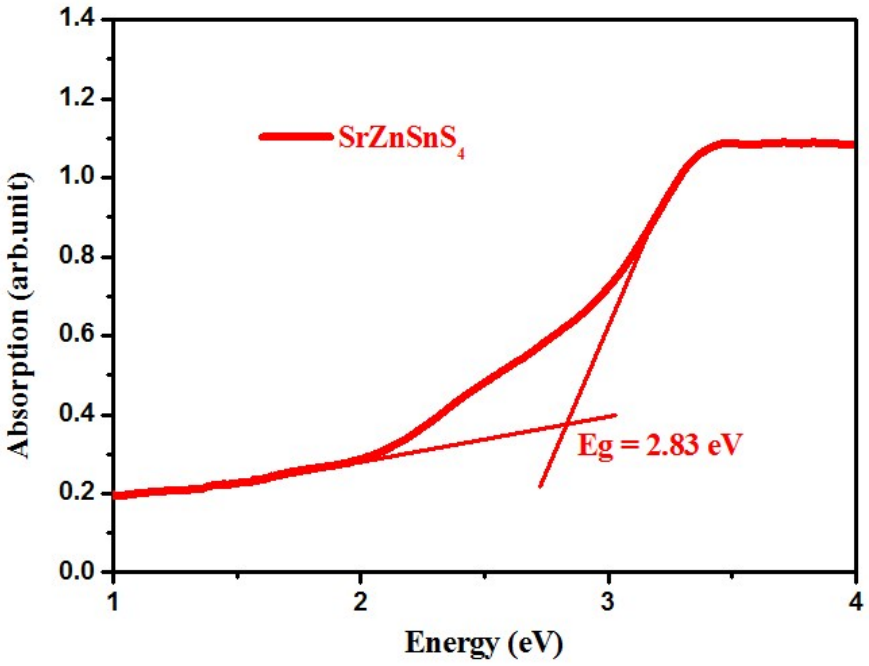

Figure S2. The experimental and simulated X-ray diffraction result of $SrZnSnS_4$ powder.

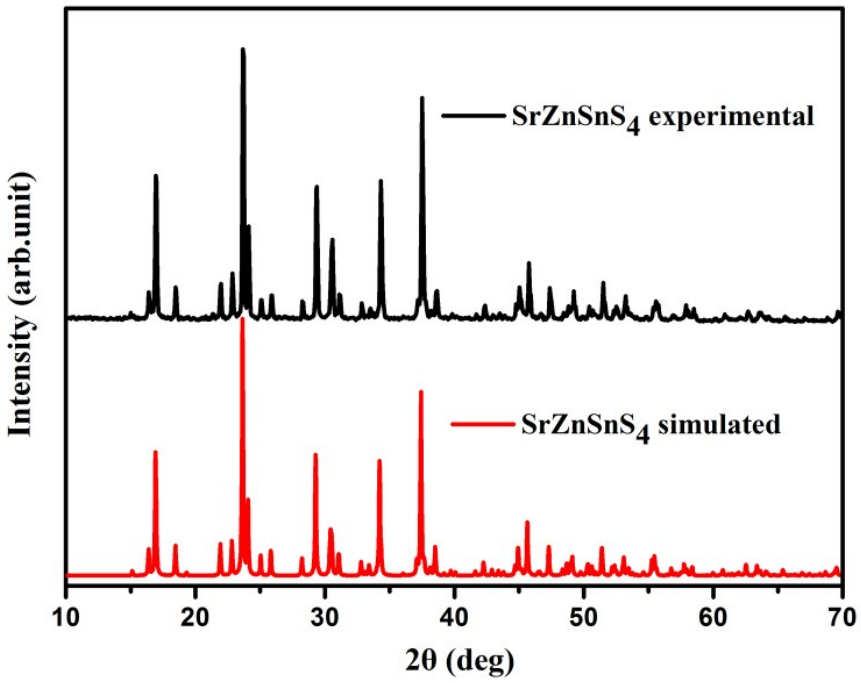

Figure S3. The SHG intensity of $SrZnSnS_4$ at 1.06 μm radiation.

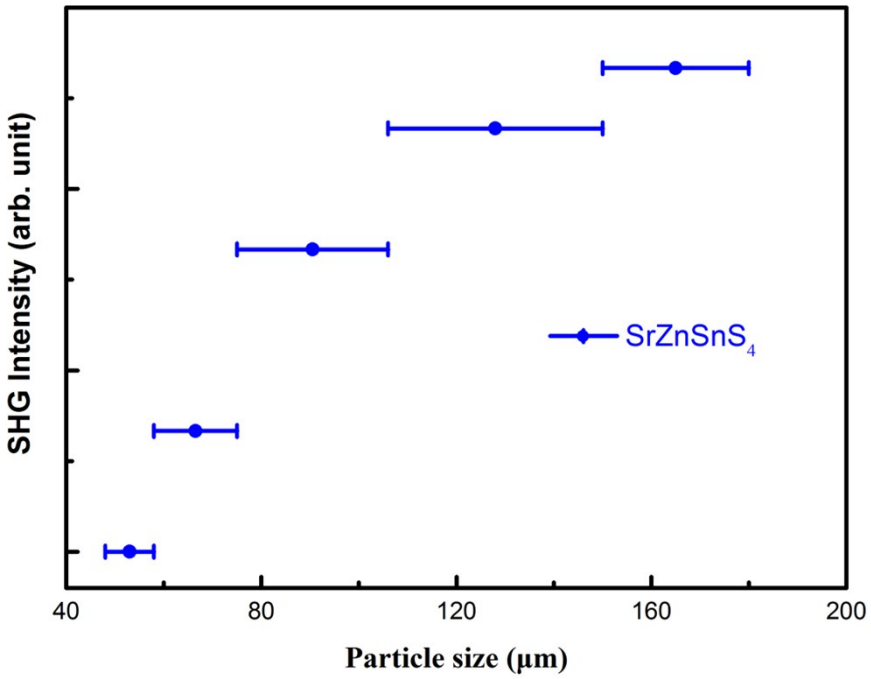

References

1. G. M. Sheldrick, *Acta Crystallogr. A*, 2008, **64**, 112–122.

2. S. K. Kurtz and T. T. Perry, *J. Appl. Phys.*, 1968, **39**, 3798–3813.

3. S. J. Clark, M. D. Segall, C. J. Pickard, P. J. Hasnip, M. J. Probert, K. Refson and M. C. Payne, *ZKri*, 2005, **220**, 567–570.

4. M. C. Payne, M. P. Teter, D. C. Allan, T. A. Arias and J. D. Joannopoulos, *Rev. Mod. Phys.*, 1992, **64**, 1045–1097.

5. H. J. Monkhorst and J. D. Pack, *Phys. Rev. B*, 1976, **13**, 5188–5192.

6. R. W. Godby, M. Schluter, L. J. Sham, *Phys. Rev. B*, 1988, **37**, 10159–10175.

7. A. M. Rappe, K. M. Rabe, E. Kaxiras and J. D. Joannopoulos, *Phys. Rev. B*, 1990, **41**, 1227–1230.

8. L. Kleinman and D. M. Bylander, *Phys. Rev. Lett.*, 1982, **48**, 1425–1428.

9. E. D. Palik, *Academic Press: New York*, 1985.

10. (a) J. Lin, M. H. Lee, Z. P. Liu, C. T. Chen and C. J. Pickard, *Phys. Rev. B*, 1999, **60**, 13380–13389; (b) Z. S. Lin, X. X. Jiang, L. Kang, P. F. Gong, S. Y. Luo and M. H. Lee, *J. Phys. D. Appl. Phys.*, 2014, **47**, 253001.

11. I. D. Brown and D. Altermatt, *Acta Crystallogr. Sect. B*, 1985, **41**, 244–247.

12. I. D. Brown, *J. Solid State Chem.*, 1989, **82**, 122–131.

13. N. E. Brese and M. O'Keeffe, *Acta Crystallogr. Sect. B*, 1991, **47**, 192–19.

14. N. Zhen, K. Wu, Y. Wang, Q. Li, W. H. Gao, D. W. Hou, Z. H. Yang, H. D. Jiang, Y. J. Dong and S. L. Pan, *Dalton Trans.*, 2016, **45**, 10681–10688.

15. Y. J. Lin, B. W. Liu, R. Ye, X. M. Jiang, L. Q. Yang, H. Y. Zeng and G. C. Guo, *J. Mater. Chem. C*, 2019, **7**, 4459–4465.

16. W. L. Yin, A. K. Iyer, C. Li, J. Y. Yao and A. Mar, *J. Alloy. Compd.*, 2017, **708**, 414–421.

17. K. Wu, X. Su, Z. H. Yang and S. L. Pan, *Dalton Trans.,* 2015, **44**, 19856–19864.

18. Y. W. Dou, Y. Chen, Z. Li, A. K. Iyer, B. Kang, W. L. Yin, J. Y. Yao and A. Mar, *Cryst. Growth Des.*, 2019, **19**, 1206–1214.

19. Y. W. Guo, F. Liang, W. L. Yin, Z. Li, X. Y. Luo, Z. S. Lin, J. Y. Yao, A. Mar and Y. C. Wu, *Chem. Mater*., 2019, **31**, 3034–3040.